
Causal Mediation Analysis with Multi-dimensional and Indirectly Observed Mediators

Ziyang Jiang¹ Yiling Liu¹ Michael H. Klein¹ Ahmed Aloui¹ Yiman Ren²
Keyu Li¹ Vahid Tarokh¹ David Carlson¹

¹Duke University ²University of Michigan Ross School of Business
{ziyang.jiang,yiling.liu,michael.klein413,ahmed.aloui,keyu.li,
vahid.tarokh,david.carlson}@duke.edu
yimanren@umich.edu

Abstract

Causal mediation analysis (CMA) is a powerful method to dissect the total effect of a treatment into direct and mediated effects within the potential outcome framework. This is important in many scientific applications to identify the underlying mechanisms of a treatment effect. However, in many scientific applications the mediator is unobserved, but there may exist related measurements. For example, we may want to identify how changes in brain activity or structure mediate an antidepressant’s effect on behavior, but we may only have access to electrophysiological or imaging brain measurements. To date, most CMA methods assume that the mediator is one-dimensional and observable, which oversimplifies such real-world scenarios. To overcome this limitation, we introduce a CMA framework that can handle complex and indirectly observed mediators based on the identifiable variational autoencoder (iVAE) architecture. We prove that the true joint distribution over observed and latent variables is identifiable with the proposed method. Additionally, our framework captures a disentangled representation of the indirectly observed mediator and yields accurate estimation of the direct and mediated effects in synthetic and semi-synthetic experiments, providing evidence of its potential utility in real-world applications.

1 Introduction

Causal inference methods are powerful tools to understand and quantify the causal relationships between treatments and outcomes, motivating studies in many areas [1–4]. Causal inference has been combined with machine learning in recent years to make powerful and flexible frameworks [5, 6]. While these frameworks are highly useful to estimate the total treatment effect on an outcome, many scientific applications require understanding *how* a treatment impacts outcomes. This knowledge can then be used to design interventions that target the mediators to influence the outcome of interest. For example, we may want to identify neural changes that mediate a behavioral outcome when studying a treatment for a psychiatric disorder. Recent work has in fact found and *manipulated* neural changes related to depression [7] and social processing [8].

This need motivates the usage of *causal mediation analysis* (CMA), which estimates the causal effect on an outcome of interest that is due to changes in intermediate variables (the “mediators”) versus directly from the treatment [9]. In specific contexts, understanding the role of the mediator is crucial as it tells us how nature works and provides insights into the underlying mechanisms that link variables, which enables a more accurate assessment of the treatment’s effectiveness. In the above case, this means estimating how much of the behavior change is explained by the treatment’s impact on the brain, as well as how much behavioral change is unexplained by that relationship. Early studies

on mediation analysis mainly adopted linear structural equation models (SEMs) including Wright’s method of path analysis [10, 11] and Baron and Kenny’s method for testing mediation hypotheses [12]. In the past few decades, researchers have come up with nonparametric generalizations for SEMs [13, 14] which do not impose any functional or distributional forms on the causal relationships and therefore offer greater flexibility in modeling complex dependencies between variables.

Despite these advances, a key challenge is that causal mediation analysis typically assumes a low-dimensional, often one-dimensional, mediator, whereas in many cases we want to identify mediation effects of complex data, such as neuroimaging, electrophysiology, and myriad -omics studies. In this paper, we build upon the concept of the identifiable variational autoencoder (iVAE) [15] and introduce a novel framework for CMA that can handle *multi-dimensional* and *indirectly observed* mediators. We assume that there is a latent space that generates the high-dimensional observed data (e.g., a smaller latent space can generate the observed neural dynamics). By using an identifiable model structure, we show that we can recover the latent space prior conditioned on the treatment and any available covariates. In summary, our main contributions are:

- We propose a causal graph that involves both an *indirectly observed* mediator and observed covariates that acts as a confounder for the treatment, the mediator, and the outcome.
- We build a framework for CMA that can handle *multi-dimensional* and *indirectly observed* mediators based on the proposed causal graph.
- We theoretically prove that the joint distribution over observed and latent variables in our framework is identifiable.
- We show that our framework learns a disentangled representation of the *indirectly observed* mediator between control and treatment groups.
- We empirically demonstrate the effectiveness of our framework on complex synthetic and semi-synthetic datasets.

2 Related Work

Causal Mediation Analysis As mentioned in the introduction, traditional mediation analysis was mainly based on linear SEMs where the direct, mediated, and total effects are determined by linear regression coefficients [10–12, 16, 17]. Despite its simplicity, this approach relies on several assumptions such as normally distributed residuals [18] and often leads to ambiguities when either the mediator or the outcome variable is not continuous [19]. To address this limitation, researchers formulated the causal mediation analysis (CMA) framework based on counterfactual thinking [9, 20, 21], which can accommodate nonlinear or nonparametric models such as targeted maximum likelihood estimation [22], inverse propensity weighting (IPW) [23], and natural effect models (NEMs) [24]. Within the counterfactual framework, the causal effects are calculated as the difference between two counterfactual combinations of mediators and outcomes, for which we will provide formal definitions in the next section. Although causal effects are defined at the individual level, in practice, we usually relax our estimation to their expected values over the population as we do not generally observe both potential outcomes simultaneously [25].

Causal Mediation Effect Estimation with Deep Models Deep learning models have gained increasing attention for their capability in estimating causal effects within the potential outcome framework [26–29]. In contrast, the use of deep learning models for mediation effect estimation has received comparatively less exploration. Xu et al. [30] developed a semiparametric neural network-based framework to reduce the bias in CMA. Cheng et al. [31] and Xu et al. [32] used variational autoencoders (VAEs) to estimate the mediation effect based on a causal graph with hidden confounders. Although these VAE-based methods share some similarities with our proposed method, we distinguish ourselves by modeling the *mediator* as the latent variable rather than the covariates, resulting in a different causal graph. Furthermore, these approaches assume that the mediator is observable and one-dimensional, which is not necessarily the case in many scientific applications.

Multi-dimensional Mediators Compared to the many CMA methods proposed, significantly less research has been conducted on scenarios where the mediator is multi-dimensional and not directly observable. The majority of investigations on this subject are situated within the domains of neuroscience [33, 34], biostatistics [35], and bioinformatics [36–39]. The approach proposed by Nath

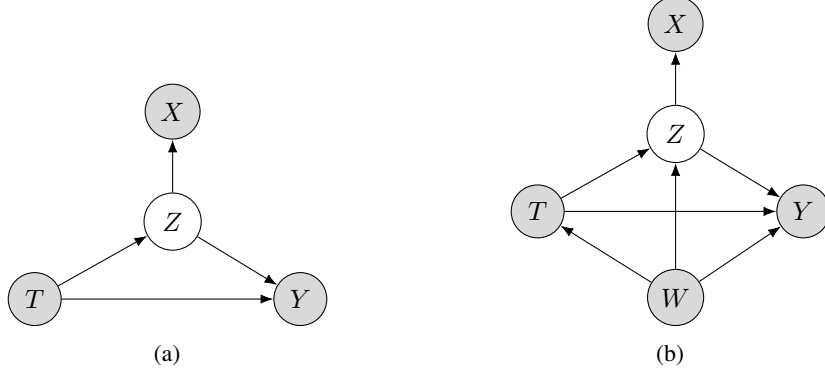


Figure 1: Graphs of CMA for (a) case without observed covariates and (b) case with observed covariates, where T is the treatment assignment, Y is the outcome, Z is the unobserved true mediator, W is a set of observed covariates, and X is a feature caused by the unobserved true mediator Z with a much higher dimension. The observed variables are colored in grey.

et al. [34] is the most relevant work to our research, where the high-dimensional mediator is first transformed into a one-dimensional variable, and the mediation effect is estimated using an iterative maximization algorithm. Nevertheless, all these methods primarily rely on linear SEMs and neglect the impact of any confounding variables, thereby limiting their applicability.

3 Problem Setup

We assume that our causal model belongs to one of the two cases as displayed in Figure 1. To ensure consistency with previous studies on mediation analysis [18, 40, 41], we further assume that the treatment assignment T is binary for each observed samples, with $T = 0$ indicating an assignment to the control group and $T = 1$ indicating an assignment to the treatment group. Consider the n^{th} individual in an experiment with a total of N units (i.e. $n = 1, \dots, N$). Let $z_n(t_n) \in \mathcal{Z} \subset \mathbb{R}^d$ denote the potential value of the unobserved true mediator under the treatment assignment t_n . Since Y depends on both T and Z , we denote $y(t_n, z_n(t_n)) \in \mathcal{Y} \subset \mathbb{R}$ as the potential outcome of the n^{th} individual under treatment t_n and true mediator $z_n(t_n)$. Following [9, 40, 42], we can define the average causal mediation effects (ACME), the average direct effects (ADE), and the average total effect (ATE) as follows:

$$ACME(t) := \mathbb{E}[y(t, z(1)) - y(t, z(0))], \quad (1)$$

$$ADE(t) := \mathbb{E}[y(1, z(t)) - y(0, z(t))], \quad (2)$$

$$ATE := \mathbb{E}[y(1, z(1)) - y(0, z(0))], \quad (3)$$

where the expectations are taken over all the samples in our experiment. Our main objective is to recover these quantities as accurately as possible. As z_n is unobserved, we must infer z_n from the related observed feature $x_n \in \mathcal{X} \subset \mathbb{R}^D$ with a much higher dimension, i.e. $D \gg d$, as well as any other available information. In practice, there often exists a set of observed covariates $w_n \in \mathcal{W} \subset \mathbb{R}^m$ that also acts as confounders for T , Z , and Y as shown in Figure 1b. With the presence of observed covariates, we need to make the following assumptions to make valid inferences about the causal effects:

Assumption 3.1. There exists an observed variable $X \in \mathcal{X} \subset \mathbb{R}^D$ that is caused by the unobserved true mediator $Z \in \mathcal{Z} \subset \mathbb{R}^d$ as shown in Figure 1.

Assumption 3.2. The following two conditional independence assumptions hold sequentially.

$$\{Y(t', z), Z(t)\} \perp\!\!\!\perp T | W = w, \quad (4)$$

$$Y(t', z) \perp\!\!\!\perp Z(t) | T = t, W = w, \quad (5)$$

where $0 < p(T = t | W = w) < 1$, $0 < p(Z(t) = z | T = t, W = w) < 1$, and $t, t' \in \{0, 1\}$.

Assumption 3.2 is first introduced by Imai et al. [3], which is also known as *sequential ignorability*. Note that Equation 4 is equivalent to the strong ignorability assumption common in causal inference

[43, 44]. It states that the treatment assignment T is statistically independent of potential outcome Y and potential mediators Z given covariates W . Equation 5 states that given the treatment and covariates, the mediator Z can be viewed as if it was randomized (in other words, there are no explained “backdoor” paths between the mediator and outcome [18]).

4 Method

We leverage the model structure of identifiable variational autoencoder (iVAE) to estimate the causal mediation effects based on the causal graphs illustrated in Figure 1. Our primary objective is to learn a disentangled representation of the true mediator in the latent space so that the statistical distance between $p(z|t = 0)$ and $p(z|t = 1)$ can be better estimated. In the following sections, we briefly review the concepts of identifiable variational autoencoder (iVAE) in Section 4.1, present our framework in Section 4.2, and formally state the identifiability of our framework in Section 4.3.

4.1 Identifiable Variational Autoencoder (iVAE)

To begin with, here we provide a brief overview of iVAE [15]. We abuse the notation slightly by redefining \mathbf{x} and \mathbf{z} to refer to the observed data and the latent feature learned by a general variational autoencoder (VAE), respectively. The primary claim made by iVAE is that a VAE becomes identifiable up to a *linear invertible transformation* (see Section 4.3 for full definitions) if we introduce a factorized prior distribution over the latent variable \mathbf{z} conditioned on an auxiliary variable \mathbf{u} . Specifically, we have \mathbf{z} sampled from $p(\mathbf{z}|\mathbf{u})$ which is assumed to be conditionally factorial with each $z_i \in \mathbf{z}$ belonging to a univariate exponential family as specified by the following probability density function:

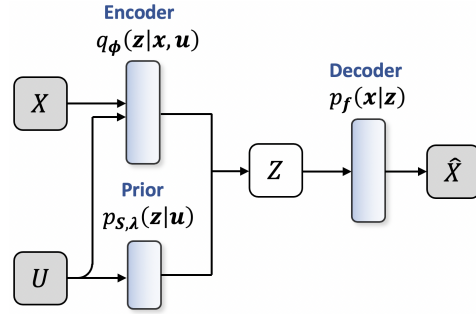


Figure 2: Illustration of an iVAE where the blue nodes correspond to probabilistic distributions.

$$p_{\mathbf{S}, \boldsymbol{\lambda}}(\mathbf{z}|\mathbf{u}) = \prod_i \frac{Q_i(z_i)}{C_i(\mathbf{u})} \exp \left[\sum_{j=1}^k S_{i,j}(z_i) \lambda_{i,j}(\mathbf{u}) \right], \quad (6)$$

where Q_i is the base measure, $C_i(\mathbf{u})$ is the normalizing constant, k is a pre-defined number of sufficient statistics, $\mathbf{S}_i = (S_{i,1}, \dots, S_{i,k})$ are the sufficient statistics, and $\boldsymbol{\lambda}_i(\mathbf{u}) = (\lambda_{i,1}(\mathbf{u}), \dots, \lambda_{i,k}(\mathbf{u}))$ are the natural parameters.

The architecture of the iVAE framework is displayed in Figure 2, which consists of a variational posterior $q_\phi(\mathbf{z}|\mathbf{x}, \mathbf{u})$ and a conditional generative model $p_\theta(\mathbf{x}, \mathbf{z}|\mathbf{u}) = p_{\mathbf{f}}(\mathbf{x}|\mathbf{z})p_{\mathbf{S}, \boldsymbol{\lambda}}(\mathbf{z}|\mathbf{u})$ where \mathbf{f} is an injective function such that $p_{\mathbf{f}}(\mathbf{x}|\mathbf{z}) = p_\epsilon(\mathbf{x} - \mathbf{f}(\mathbf{z}))$ and ϵ is an independent noise variable with probability density function $p(\epsilon)$. The parameters of the generative model are denoted as $\boldsymbol{\theta} = \{\mathbf{f}, \mathbf{S}, \boldsymbol{\lambda}\}$. When fitting iVAE on observed data, the parameter vector $(\boldsymbol{\theta}, \phi)$ is learned by maximizing the evidence lower bound (ELBO) $\mathcal{L}_{\boldsymbol{\theta}, \phi}(\mathbf{x}, \mathbf{u})$:

$$\log p_\theta(\mathbf{x}|\mathbf{u}) \geq \mathcal{L}_{\boldsymbol{\theta}, \phi}(\mathbf{x}, \mathbf{u}) := \mathbb{E}_{q_\phi(\mathbf{z}|\mathbf{x}, \mathbf{u})} [\log p_\theta(\mathbf{x}, \mathbf{z}|\mathbf{u}) - \log q_\phi(\mathbf{z}|\mathbf{x}, \mathbf{u})], \quad (7)$$

where we use the reparameterization trick to sample from $q_\phi(\mathbf{z}|\mathbf{x}, \mathbf{u})$. Briefly speaking, both the model structure and the learning process of iVAE are similar to conventional VAEs except that the prior, the variational posterior, and the decoder are additionally conditioned on the auxiliary variable \mathbf{u} . However, it is important to note that \mathbf{u} must have some association with \mathbf{x} and \mathbf{z} .

4.2 Estimating Mediation Effect with VAE

In this section, we formally present our approach — Identifiable Mediation Analysis with Variational Autoencoder (IMAVAE), with the overall architecture displayed in Figure 3. The encoder, decoder, and prior components in IMAVAE have exactly the same probabilistic form as specified in Section 4.1 and share a similar structure with iVAE, where we take the high-dimensional feature X as the input to the encoder to learn the unobserved mediator Z and generate a reconstruction \hat{X} with the

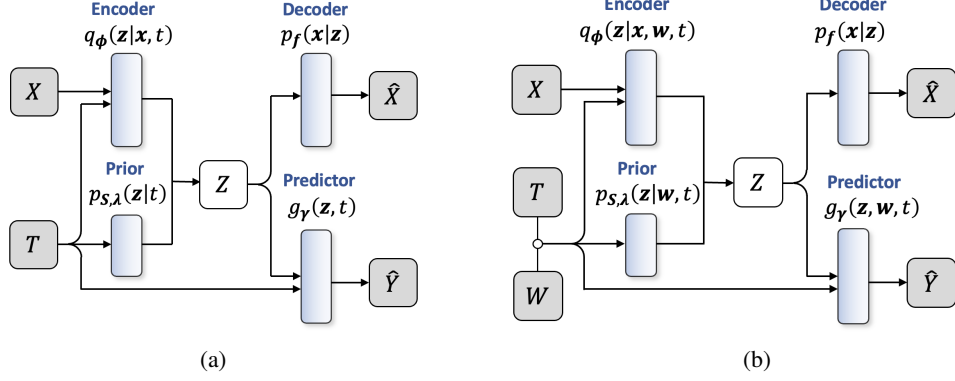


Figure 3: Illustration of the overall architecture of IMAVAE for (a) case without observed covariates and (b) case with observed covariates. Note that in case (b) the treatment assignment T and the observed covariates W are first concatenated and then passed into the prior, encoder, and decoder.

decoder. Importantly, we further include a parametric model g_γ to predict the outcome \hat{Y} . Figures 3a and 3b depict two variants of our framework, corresponding to the two cases outlined in the causal graphs in Figure 1:

- *Case (a)*: Without observed covariates, the treatment assignment T is employed as the auxiliary variable and serves as input to the encoder, prior, and predictor, as illustrated in Figure 3a.
- *Case (b)*: With observed covariates, we first concatenate the observed covariates W and the treatment assignment T . The concatenated vector (W, T) is then passed into the encoder, prior, and predictor as the auxiliary variable, as illustrated in Figure 3b.

Similar to iVAE, we denote the parameter vector of IMAVAE as (θ, ϕ, γ) where $\theta = \{\mathbf{f}, \mathbf{S}, \lambda\}$. When fitting IMAVAE to the observed data, we optimize the parameter vector by minimizing the following objective:

$$\theta^*, \phi^*, \gamma^* := \arg \min_{\theta, \phi, \gamma} \{ \alpha \mathcal{L}_{\theta, \phi}(\hat{\mathbf{x}}, \mathbf{x}) - \beta \mathcal{L}_{\theta, \phi}(\mathbf{x}, \mathbf{u}) + \mathcal{L}_{\phi, \mathbf{S}, \lambda, \gamma}(\hat{y}, y) \}, \quad (8)$$

where $\mathbf{u} = t$ for case (a), $\mathbf{u} = (\mathbf{w}, t)$ for case (b), $\mathcal{L}_{\theta, \phi}(\hat{\mathbf{x}}, \mathbf{x})$ is the discrepancy between the input feature \mathbf{x} and its reconstruction $\hat{\mathbf{x}}$, $\mathcal{L}_{\phi, \mathbf{S}, \lambda, \gamma}(\hat{y}, y)$ is the error between the predicted outcome \hat{y} and the true outcome y . $\mathcal{L}_{\theta, \phi}(\mathbf{x}, \mathbf{u})$ represents the same loss term as Equation 7. We note that this creates some overlap as the reconstruction term on \mathbf{x} is also in Equation 7, but choose this form to highlight each term independently (and does not change the overall loss with appropriately chosen weights). α and β are hyperparameters representing the importance of the reconstruction error and the ELBO, respectively. In our experiments, we use mean squared error (MSE) loss for both $\mathcal{L}_{\theta, \phi}(\hat{\mathbf{x}}, \mathbf{x})$ and $\mathcal{L}_{\phi, \mathbf{S}, \lambda, \gamma}(\hat{y}, y)$. The prior $p_{\mathbf{S}, \lambda}(z|\mathbf{u})$ is set to be a multivariate normal distribution whose mean and covariance are parameterized as a function of \mathbf{u} using a neural network.

To give an estimation on the direct, mediated, and total effects after fitting the parameters, we repeatedly sample $z(t)$ from the learned distributions (i.e., $p_{\mathbf{S}, \lambda}(z|t)$ for case (a) and $p_{\mathbf{S}, \lambda}(z|\mathbf{w}, t)$ for case (b)). Next, we feed both $z(t)$ and the auxiliary variables into the predictor g_γ to obtain $y(t, z(t))$ for case (a) or $y(t, \mathbf{w}, z(t))$ for case (b). Finally, we estimate the ACME, ADE, and ATE according to Equations 1-3 using estimated values of y .

4.3 Identifiability of IMAVAE

In this section, we use similar definitions and assumptions stated by Khemakhem et al. [15]. Specifically, let $\mathcal{Z} \subset \mathbb{R}^d$ be the support of distribution of z . The support of distribution of \mathbf{u} is $\mathcal{U} = \{0, 1\}$ for case (a) and $\mathcal{U} = \{0, 1\} \times \mathcal{W} \subset \mathbb{R}^{m+1}$ for case (b). We denote by $\mathbf{S} := (\mathbf{S}_1, \dots, \mathbf{S}_d) = (S_{1,1}, \dots, S_{d,k}) \in \mathbb{R}^{dk}$ the vector of sufficient statistics of Equation 6 and $\lambda(\mathbf{u}) = (\lambda_1(\mathbf{u}), \dots, \lambda_d(\mathbf{u})) = (\lambda_{1,1}(\mathbf{u}), \dots, \lambda_{d,k}(\mathbf{u})) \in \mathbb{R}^{dk}$ the vector of its parameters. Following the same notations in [15], we define $\mathcal{X} \subset \mathbb{R}^D$ as the image of \mathbf{f} in Equation 6 and denote by $\mathbf{f}^{-1} : \mathcal{X} \rightarrow \mathcal{Z}$ the inverse of \mathbf{f} . Furthermore, we make the following assumption on the predictor:

Assumption 4.1. The predictor $g_\gamma(z, \mathbf{u})$ takes the following form:

$$g_\gamma(z, \mathbf{u}) := p_{\mathbf{h}}(y|z, \mathbf{u}) = p_{\xi}(y - \mathbf{h}(z, \mathbf{u})), \quad (9)$$

where the function $\mathbf{h} : \mathcal{Z} \times \mathcal{U} \rightarrow \mathcal{Y}$ is injective, $\mathcal{Y} \subset \mathbb{R}$ is the image of \mathbf{h} , and ξ is an independent noise variable with probability density function $p_{\xi}(\xi)$.

Similar to [15], for the sake of analysis, we treat \mathbf{h} as a parameter of the entire model and define $\psi := (\mathbf{f}, \mathbf{h}) : \mathcal{Z} \times \mathcal{U} \rightarrow \mathcal{X} \times \mathcal{Y}$. ψ remains injective since both \mathbf{f} and \mathbf{h} are injective, and we consider the projection ψ^{-1} on \mathcal{Z} to be $\psi|_{\mathcal{Z}}^{-1}$. The domain of parameters is thus $\Theta = \{\theta := (\mathbf{f}, \mathbf{h}, \mathbf{S}, \lambda)\}$. To formally present our claim, we give the following definitions:

Definition 4.2. Let \sim be an equivalence relation on Θ . We say that $p_\theta(x, z, y|\mathbf{u})$ is identifiable up to \sim if $p_\theta(x, z, y|\mathbf{u}) = p_{\tilde{\theta}}(x, z, y|\mathbf{u}) \implies \theta \sim \tilde{\theta}$.

Definition 4.3. Let \sim_A be the equivalence relation on Θ defined as follows:

$$(\mathbf{f}, \mathbf{h}, \mathbf{S}, \lambda) \sim (\tilde{\mathbf{f}}, \tilde{\mathbf{h}}, \tilde{\mathbf{S}}, \tilde{\lambda}) \iff \exists A, \mathbf{c} | \mathbf{S}(\psi|_{\mathcal{Z}}^{-1}(x, y)) = A\tilde{\mathbf{S}}(\tilde{\psi}|_{\mathcal{Z}}^{-1}(x, y)) + \mathbf{c}, \forall x \in \mathcal{X}; y \in \mathcal{Y}, \quad (10)$$

where A is an invertible $dk \times dk$ matrix and \mathbf{c} is a vector.

With all the assumptions and definitions stated above, we state our theorem below as an extension of the results in [15]. The detailed proof will be provided in Appendix A.

Theorem 4.4. (Extension to Theorem 1 in Khemakhem et al. [15]) Assume that we observe data sampled from the generative model $p_\theta(x, z, y|\mathbf{u}) = p_f(x|z)p_h(y|z, \mathbf{u})p_{S, \lambda}(z|\mathbf{u})$ where $p_f(x|z)$, $p_h(y|z, \mathbf{u})$ and $p_{S, \lambda}(z|\mathbf{u})$ follow the distributional form defined in Section 4.1, Equation 9, and Equation 6, respectively. Then the parameters $(\mathbf{f}, \mathbf{h}, \mathbf{S}, \lambda)$ will be \sim_A -identifiable if we assume the following holds:

1. The set $\{(x, y) \in \mathcal{X} \times \mathcal{Y} | \varphi_\epsilon(x) = 0, \varphi_\xi(y) = 0\}$ has measure zero, where φ_ϵ and φ_ξ are the characteristic functions of p_ϵ and p_ξ defined in Section 4.1 and Equation 9, respectively.
2. The functions f and h are both injective.
3. The sufficient statistics $S_{i,j}$ in Equation 6 are differentiable almost everywhere, and $(S_{i,j})_{1 \leq j \leq k}$ are linearly independent on any subset of \mathcal{Y} of measure greater than zero.
4. There exists $dk + 1$ distinct points $\mathbf{u}_0, \dots, \mathbf{u}_{dk}$ such that the matrix $L = (\lambda(\mathbf{u}_1) - \lambda(\mathbf{u}_0), \dots, \lambda(\mathbf{u}_{dk}) - \lambda(\mathbf{u}_0))$ of size $dk \times dk$ is invertible.

With the aforementioned theorem, we state that the joint distribution learned by the generative model $p_\theta(x, z, y|\mathbf{u})$ is identifiable. Moreover, it is important to highlight that our extension of the identifiability theorem, originally presented in [15], incorporates the additional conditioning of y on \mathbf{u} , thereby broadening the scope of iVAE.

5 Experiments

We follow the approach using synthetic and semi-synthetic datasets used in recent causal inference manuscripts to allow for benchmarking and comparison of the results. We test IMAVAE on 3 datasets: 1 synthetic dataset and 2 semi-synthetic datasets¹. This allows us to evaluate how well we estimate counterfactual values of the treatment assignment and the mediator, and the direct, mediated, and total effects under reasonable assumptions. The detailed experimental setup (e.g. training details, computing resources, licenses, etc.) is given in Appendix B.

5.1 Synthetic Dataset

We first construct a synthetic dataset following the causal graphs in Figure 1, where we give the details of data generation process in Appendix C. We set the unobserved true mediator to be two-dimensional (i.e. $d = 2$) for easier visualization. We display the distributions of the true and estimated unobserved mediator in Figure 4, where we note that IMAVAE effectively learns *disentangled representations*

¹Code will be released upon acceptance.

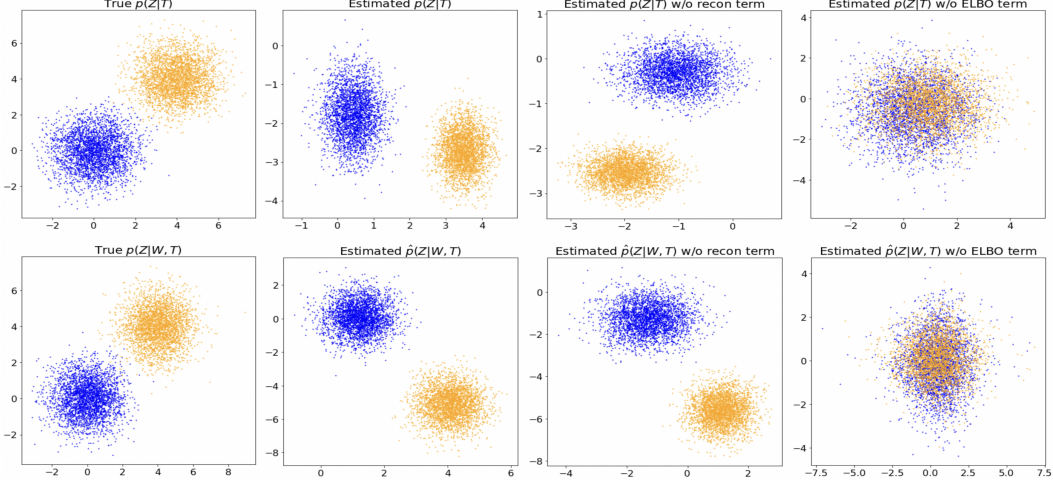


Figure 4: Distribution of the true and the estimated $p(z|\mathbf{u})$ in the latent space where the upper row corresponds to case (a) without observed covariates, i.e. $\mathbf{u} = t$ and the bottom row corresponds to case (b) with observed covariates, i.e. $\mathbf{u} = (w, t)$. From left to right, we present (left) the true distribution of $p(z|\mathbf{u})$, (middle left) the estimated distribution $\hat{p}_{S,\lambda}(z|\mathbf{u})$ by IMVAE, (middle right) the estimated distribution $\hat{p}_{S,\lambda}(z|\mathbf{u})$ without the reconstruction term, i.e. $\alpha = -1$, and (right) the estimated distribution $\hat{p}_{S,\lambda}(z|\mathbf{u})$ without the ELBO term, i.e. $\beta = 0$. The blue dots denote samples in control group and the orange dots denote samples in treatment group.

of Z for the control and treatment groups in the latent space, up to trivial indeterminacies such as rotations and sign flips, for cases both with and without observed covariates. If we remove the reconstruction term (i.e. $\alpha = -1$ due to the overlap of reconstruction terms in Equation 8), the shape and orientation of the distributions become slightly different but remain disentangled. However, if we discard the ELBO term (i.e. $\beta = 0$), the model fails to separate the distributions of control and treatment groups. We also compute the absolute errors between the estimated ACME, ADE, ATE, and their corresponding ground truths as shown in Tables 1 and 2. It can be observed that IMVAE yields slightly larger errors when the reconstruction term is removed (i.e., $\alpha = -1$). However, without the ELBO term (i.e., $\beta = 0$), the model produces significantly larger errors on ACME and ATE. From the obtained results, we conclude that the iVAE-like structure in our framework is essential for learning a better representation of the unobserved mediator, which, in turn, improves the accuracy of mediation effect estimation.

5.2 Electrophysiological Dataset

As described in the introduction, causal mediation analysis holds significant relevance for applications in systems neuroscience. Once such area is in the emerging area of targeted neurostimulation (see [45–47] for a description), where the brain is manipulated by optical, electrical, or mechanical stimulation with the goal of manipulating behavior in many brain conditions. However, while the mechanism of behavioral change is the brain, identifying such changes is challenging with existing causal mediation techniques due to the high-dimensional and complex nature of the brain data. Accurate appraisal of neural changes causing behavioral change will provide a deeper understanding of mechanisms driving neural activity and potentially lead to more efficacious treatments.

We demonstrate capability of our method to this domain with a semisynthetic dataset by post-processing real multi-site brain recordings using local field potential (LFP) data from 26 mice [48], which is publicly available [49]. Each mouse is recorded by a certain number of time steps, resulting in a total of 43,882 data points. We take the LFP signals as the observed feature X , while the true mediator Z is manually generated by applying principal component analysis (PCA) to map X into a lower-dimensional representation. The treatment assignment T indicates whether the mouse is recorded during an open field exploration ($T = 0$) or a tail suspension test ($T = 1$). Furthermore, we consider the genotype of the mouse, a binary variable, as an observed covariate, denoted by $W \in \{0, 1\}$. Lastly, we construct the outcome Y manually as a function of the treatment, the mediator, and the

Table 3: Absolute error of ACME under treated, ADE under control, and ATE on the tail suspension test dataset for IMAVAE and other benchmarks.

| | Case (a) | | | | Case (b) | | | |
|------------------|----------------------|--------------------|--------------|--------------|----------------------|--------------|-------------|-------------|
| | IMAVAE (ours) | Shallow LSEM | Deep LSEM | HIMA | IMAVAE (ours) | Shallow LSEM | Deep LSEM | HIMA |
| ACME ($t = 1$) | 2.348 ± 0.003 | 15.14 ± 0.03 | 15.48 ± 0.07 | 13.95 ± 0.03 | 0.559 ± 0.002 | 3.06 ± 2.16 | 4.80 ± 0.44 | 2.67 ± 0.02 |
| ADE ($t = 0$) | 1.603 ± 0.000 | 14.71 ± 0.03 | 15.06 ± 0.07 | 3.82 ± 0.01 | 0.782 ± 0.000 | 5.03 ± 1.20 | 5.16 ± 0.51 | 3.21 ± 0.01 |
| ATE | 0.744 ± 0.003 | 0.42 ± 0.06 | 0.42 ± 0.14 | 17.77 ± 0.03 | 0.223 ± 0.002 | 1.96 ± 3.36 | 0.36 ± 0.94 | 0.54 ± 0.02 |

genotype (only for case (b) with observed covariate). The detailed procedure of dataset generation is given in Appendix D.

We compare our method with two baseline models that are designed to handle high-dimensional mediators: an integrated framework of shallow or deep neural network and linear SEM (Shallow/Deep LSEM) [34] and a high-dimensional mediation analysis (HIMA) framework [39]. Notably, HIMA considers each component of Z as an individual mediator instead of a multidimensional mediator. As such, we report the mediation effect using the component with the highest correlation. We compute and display the absolute errors of ACME, ADE, and ATE in Table 3. Our results indicate that IMAVAE outperforms both benchmarks by a very wide margin on all estimations except the ATE in case (a) without covariates. The two benchmarks used in this experiment yield significantly larger errors on ACME and ADE. We believe this is reasonable, as both benchmarks are designed based on linear SEMs and are thus not able to capture the correlation between the components of Z .

5.3 Jobs II Dataset

To evaluate whether our method can generalize to real-world scenarios used in recent causal mediation analysis frameworks, we test IMAVAE on the Jobs II dataset [50], which aims to explore the impact of unemployment on workers’ stress and mental health and evaluate the potential benefits of participation in a job-search skills seminar. The dataset includes a binary treatment assignment T , which indicates whether a participant was assigned to attend a job-search skills seminar ($T = 1$) or to receive a booklet ($T = 0$). The mediator Z is a continuous variable that measures the job-search efficacy. All other attributes are treated as the observed covariates W . The outcome variable Y is also a continuous variable that represents the level of depression reported by each participant during follow-up interviews. To obtain the ground truth for direct and mediated effects, we followed a simulation procedure similar to [51] to make ACMEs, ADEs, and ATE all equal to zero. The detailed simulation procedure is given in Appendix E.

We compare the performance of our method with several benchmarks: nonlinear SEM with interaction (LSEM-I) [3], imputing-based natural effect model (NEM-I) [24], IPW [23], and Causal Mediation Analysis with Variational Autoencoder (CMAVAE) [31]. It is worth noting that the Jobs II dataset presents an observable mediator variable Z , which is *not* the optimal scenario for our proposed framework, as IMAVAE is specifically designed for CMA with *implicitly* observed mediators. Nonetheless, according to the results shown in Tables 4 and 5 (where N is the total number of simulated samples and η is a simulation parameter which stands for the magnitude of selection into the mediator), our

| | IMAVAE | IMAVAE $\alpha = -1$ | IMAVAE $\beta = 0$ |
|------------------|--------------|----------------------|--------------------|
| ACME ($t = 1$) | 0.056 ± .007 | 0.078 ± .007 | 2.875 ± .016 |
| ADE ($t = 0$) | 0.058 ± .000 | 0.052 ± .000 | 0.043 ± .000 |
| ATE | 0.003 ± .007 | 0.025 ± .006 | 2.917 ± .015 |

Table 1: Absolute error of ACME under treated, ADE under control, and ATE on the synthetic dataset for IMAVAE in case (a) *without* observed covariates

| | IMAVAE | IMAVAE $\alpha = -1$ | IMAVAE $\beta = 0$ |
|------------------|--------------|----------------------|--------------------|
| ACME ($t = 1$) | 0.214 ± .016 | 0.379 ± .014 | 5.912 ± .028 |
| ADE ($t = 0$) | 0.194 ± .000 | 0.385 ± .000 | 0.127 ± .000 |
| ATE | 0.019 ± .015 | 0.011 ± .016 | 6.036 ± .028 |

Table 2: Absolute error of ACME under treated, ADE under control, and ATE on the synthetic dataset for IMAVAE in case (b) *with* observed covariates

Table 4: Absolute error of ACME under treated, ADE under control, and ATE on simulated Jobs II data for IMAVAE and other benchmarks where 10% of the data are mediated (i.e. $Z > 3$).

| N | LSEM-I | | NEM-I | | IPW | | CMAVAE | | IMAAVE (ours) | |
|--------------------------------|---------------|---------------------------------|---------------------------------|---------------------------------|---------------|---------------|---------------------------------|---------------------------------|---------------------------------|---------------------------------|
| | 500 | 1000 | 500 | 1000 | 500 | 1000 | 500 | 1000 | 500 | 1000 |
| ACME under treated ($t = 1$) | | | | | | | | | | |
| $\eta = 10$ | 0.9 \pm .04 | 0.6 \pm .02 | 0.6 \pm .03 | 0.8 \pm .01 | 0.6 \pm .04 | 0.8 \pm .02 | 0.2 \pm .00 | 0.3 \pm .00 | 0.1 \pm .02 | 0.1 \pm .01 |
| $\eta = 1$ | 0.0 \pm .01 | 0.1 \pm .01 | 0.0 \pm .00 | 0.1 \pm .01 | 0.0 \pm .01 | 0.1 \pm .01 | 0.1 \pm .00 | 0.1 \pm .00 | 0.1 \pm .01 | 0.0 \pm .01 |
| ADE under control ($t = 0$) | | | | | | | | | | |
| $\eta = 10$ | 1.3 \pm .07 | 1.6 \pm .06 | 1.2 \pm .06 | 1.8 \pm .05 | 1.2 \pm .06 | 0.2 \pm .06 | 0.1 \pm .00 | 0.0 \pm .03 | 0.3 \pm .00 | 0.3 \pm .00 |
| $\eta = 1$ | 3.3 \pm .08 | 0.0 \pm .07 | 1.1 \pm .03 | 0.2 \pm .07 | 3.3 \pm .08 | 0.3 \pm .06 | 0.5 \pm .02 | 0.4 \pm .01 | 0.2 \pm .00 | 0.3 \pm .00 |
| ATE | | | | | | | | | | |
| $\eta = 10$ | 2.2 \pm .05 | 1.0 \pm .06 | 1.8 \pm .05 | 0.9 \pm .06 | 0.5 \pm .05 | 1.0 \pm .06 | 0.3 \pm .01 | 0.3 \pm .03 | 0.2 \pm .02 | 0.2 \pm .01 |
| $\eta = 1$ | 3.3 \pm .08 | 0.1 \pm .07 | 3.4 \pm .03 | 0.1 \pm .06 | 3.2 \pm .07 | 0.2 \pm .05 | 0.4 \pm .02 | 0.3 \pm .01 | 0.2 \pm .01 | 0.2 \pm .01 |

Table 5: Absolute error of ACME under treated, ADE under control, and ATE on simulated Jobs II data for IMAVAE and other benchmarks where 50% of the data are mediated (i.e. $Z > 3$).

| N | LSEM-I | | NEM-I | | IPW | | CMAVAE | | IMAAVE (ours) | |
|--------------------------------|---------------|---------------------------------|---------------|---------------|---------------|---------------------------------|---------------------------------|---------------------------------|---------------------------------|---------------------------------|
| | 500 | 1000 | 500 | 1000 | 500 | 1000 | 500 | 1000 | 500 | 1000 |
| ACME under treated ($t = 1$) | | | | | | | | | | |
| $\eta = 10$ | 0.9 \pm .03 | 0.6 \pm .03 | 0.2 \pm .03 | 0.4 \pm .03 | 0.2 \pm .03 | 0.4 \pm .03 | 0.0 \pm .00 | 0.1 \pm .00 | 0.0 \pm .05 | 0.0 \pm .03 |
| $\eta = 1$ | 0.1 \pm .01 | 0.0 \pm .01 | 0.2 \pm .00 | 0.1 \pm .01 | 0.1 \pm .01 | 0.0 \pm .01 | 0.1 \pm .00 | 0.1 \pm .00 | 0.0 \pm .05 | 0.0 \pm .03 |
| ADE under control ($t = 0$) | | | | | | | | | | |
| $\eta = 10$ | 0.6 \pm .06 | 0.1 \pm .04 | 0.1 \pm .06 | 0.1 \pm .04 | 0.7 \pm .07 | 0.2 \pm .05 | 0.3 \pm .01 | 0.1 \pm .00 | 0.1 \pm .00 | 0.1 \pm .00 |
| $\eta = 1$ | 0.1 \pm .10 | 0.3 \pm .10 | 0.1 \pm .10 | 0.3 \pm .04 | 0.3 \pm .10 | 0.2 \pm .04 | 0.1 \pm .00 | 0.1 \pm .00 | 0.1 \pm .00 | 0.1 \pm .00 |
| ATE | | | | | | | | | | |
| $\eta = 10$ | 0.3 \pm .05 | 0.8 \pm .03 | 0.1 \pm .05 | 0.5 \pm .03 | 0.9 \pm .05 | 0.2 \pm .04 | 0.3 \pm .01 | 0.0 \pm .01 | 0.1 \pm .04 | 0.1 \pm .03 |
| $\eta = 1$ | 0.1 \pm .09 | 0.3 \pm .04 | 0.3 \pm .10 | 0.3 \pm .04 | 0.2 \pm .10 | 0.2 \pm .04 | 0.0 \pm .01 | 0.2 \pm .01 | 0.1 \pm .04 | 0.1 \pm .03 |

method still mostly outperforms the benchmarks in terms of the estimation on ACME, ADE, and ATE with a reasonable level of uncertainty.

6 Discussion

Design Choice of the Predictor In Section 4.3, we prove that the true joint distribution over observed and latent variables learned by IMAVAE is identifiable if we specify the predictor g_γ to be a conditional distribution reparameterized by function \mathbf{h} . However, in practice, g_γ can be as simple as a linear or logistic regression model since we believe the identifiability on $(\mathbf{f}, \mathbf{S}, \boldsymbol{\lambda})$ is enough to disentangle the representations between control and treatment groups and give an accurate estimation on the mediation effects. We encourage readers to consider designing g_γ in order to achieve optimal performance.

Limitations As discussed in Section 3, our method relies on sequential ignorability, a condition that is not directly testable using the observed data. However, recent studies [31, 32] propose a potential solution by considering X as a proxy variable and accounting for hidden confounders. Exploring this approach represents an intriguing direction for our future research.

Applications and Broader Impacts We believe the proposed model architecture can be very useful for improving interpretability for neuroscience applications. For instance, the disentangled mediator representations obtained by IMAVAE can be used to investigate the brain activities of individuals under different interventions. It can also be combined with other interpretable methods such as linear factor models to better illustrate the high-dimensional dynamics in brain networks as proposed by Talbot et al [52]. We have not identified any potential negative societal consequences specific to this manuscript.

7 Conclusion

This work makes a contribution to the field of causal mediation analysis (CMA) by proposing a novel method, IMAVAE, that can handle situations where the mediator is indirectly observed and observed covariates are likely to be present. Our approach builds on existing CMA methods and

leverages the identifiable variational autoencoder (iVAE) model architecture to provide a powerful tool for estimating direct and mediated effects. We have demonstrated the effectiveness of IMAVAE in mediation effect estimation through theoretical analysis and empirical evaluations. Specifically, we have proved the identifiability of the joint distribution learned by IMAVAE and demonstrated the disentanglement of mediators in control and treatment groups. Overall, our proposed method offers a promising avenue for CMA in settings with much more complex data, where traditional methods may struggle to provide accurate estimates.

References

- [1] Susan Athey and Guido W Imbens. The state of applied econometrics: Causality and policy evaluation. *Journal of Economic perspectives*, 31(2):3–32, 2017.
- [2] Thomas A Glass, Steven N Goodman, Miguel A Hernán, and Jonathan M Samet. Causal inference in public health. *Annual review of public health*, 34:61–75, 2013.
- [3] Kosuke Imai, Luke Keele, and Dustin Tingley. A general approach to causal mediation analysis. *Psychological methods*, 15(4):309, 2010.
- [4] Kenneth J Rothman and Sander Greenland. Causation and causal inference in epidemiology. *American journal of public health*, 95(S1):S144–S150, 2005.
- [5] Ruocheng Guo, Lu Cheng, Jundong Li, P Richard Hahn, and Huan Liu. A survey of learning causality with data: Problems and methods. *ACM Computing Surveys (CSUR)*, 53(4):1–37, 2020.
- [6] Zongyu Li and Zhenfeng Zhu. A survey of deep causal model. *arXiv preprint arXiv:2209.08860*, 2022.
- [7] Rainbo Hultman, Kyle Ulrich, Benjamin D. Sachs, Cameron Blount, David E. Carlson, Nkemdilim Ndubuizu, Rosemary C. Bagot, Eric M. Parise, Mai-Anh T. Vu, Neil M. Gallagher, Joyce Wang, Alcino J. Silva, Karl Deisseroth, Stephen D. Mague, Marc G. Caron, Eric J. Nestler, Lawrence Carin, and Kafui Dzirasa. Brain-wide electrical spatiotemporal dynamics encode depression vulnerability. *Cell*, 173(1):166–180.e14, 2018. ISSN 0092-8674. doi: <https://doi.org/10.1016/j.cell.2018.02.012>. URL <https://www.sciencedirect.com/science/article/pii/S0092867418301569>.
- [8] Stephen D. Mague, Austin Talbot, Cameron Blount, Kathryn K. Walder-Christensen, Lara J. Duffney, Elise Adamson, Alexandra L. Bey, Nkemdilim Ndubuizu, Gwenaëlle E. Thomas, Dalton N. Hughes, Yael Grossman, Rainbo Hultman, Saurabh Sinha, Alexandra M. Fink, Neil M. Gallagher, Rachel L. Fisher, Yong-Hui Jiang, David E. Carlson, and Kafui Dzirasa. Brain-wide electrical dynamics encode individual appetitive social behavior. *Neuron*, 110(10):1728–1741.e7, 2022. ISSN 0896-6273. doi: <https://doi.org/10.1016/j.neuron.2022.02.016>. URL <https://www.sciencedirect.com/science/article/pii/S0896627322001817>.
- [9] Judea Pearl. Direct and indirect effects. *Probabilistic and Causal Inference: The Works of Judea Pearl*, page 373, 2001.
- [10] Sewall Wright. The theory of path coefficients a reply to niles’s criticism. *Genetics*, 8(3):239, 1923.
- [11] Sewall Wright. The method of path coefficients. *The annals of mathematical statistics*, 5(3):161–215, 1934.
- [12] Reuben M Baron and David A Kenny. The moderator–mediator variable distinction in social psychological research: Conceptual, strategic, and statistical considerations. *Journal of personality and social psychology*, 51(6):1173, 1986.
- [13] Alexander Balke and Judea Pearl. Counterfactuals and policy analysis in structural models. *arXiv preprint arXiv:1302.4929*, 2013.
- [14] Karl G Jöreskog, Fan Yang, G Marcoulides, and R Schumacker. Nonlinear structural equation models: The kenny-judd model with interaction effects. *Advanced structural equation modeling: Issues and techniques*, 3:57–88, 1996.

- [15] Ilyes Khemakhem, Diederik Kingma, Ricardo Monti, and Aapo Hyvarinen. Variational autoencoders and nonlinear ica: A unifying framework. In *International Conference on Artificial Intelligence and Statistics*, pages 2207–2217. PMLR, 2020.
- [16] David P MacKinnon. *Introduction to statistical mediation analysis*. Routledge, 2012.
- [17] David P MacKinnon and James H Dwyer. Estimating mediated effects in prevention studies. *Evaluation review*, 17(2):144–158, 1993.
- [18] Judea Pearl. Interpretation and identification of causal mediation. *Psychological methods*, 19(4):459, 2014.
- [19] Judith JM Rijnhart, Jos WR Twisk, Iris Eekhout, and Martijn W Heymans. Comparison of logistic-regression based methods for simple mediation analysis with a dichotomous outcome variable. *BMC medical research methodology*, 19:1–10, 2019.
- [20] Paul W Holland. Causal inference, path analysis and recursive structural equations models. *ETS Research Report Series*, 1988(1):i–50, 1988.
- [21] Donald B Rubin. Estimating causal effects of treatments in randomized and nonrandomized studies. *Journal of educational Psychology*, 66(5):688, 1974.
- [22] Wenjing Zheng and Mark J van der Laan. Targeted maximum likelihood estimation of natural direct effects. *The international journal of biostatistics*, 8(1):1–40, 2012.
- [23] Martin Huber, Michael Lechner, and Conny Wunsch. The performance of estimators based on the propensity score. *Journal of Econometrics*, 175(1):1–21, 2013.
- [24] Theis Lange, Stijn Vansteelandt, and Maarten Bekaert. A simple unified approach for estimating natural direct and indirect effects. *American journal of epidemiology*, 176(3):190–195, 2012.
- [25] Paul W Holland. Statistics and causal inference. *Journal of the American statistical Association*, 81(396):945–960, 1986.
- [26] Ahmed M Alaa and Mihaela Van Der Schaar. Bayesian inference of individualized treatment effects using multi-task gaussian processes. *Advances in neural information processing systems*, 30, 2017.
- [27] Ziyang Jiang, Zhuoran Hou, Yiling Liu, Yiman Ren, Keyu Li, and David Carlson. Estimating causal effects using a multi-task deep ensemble. *arXiv preprint arXiv:2301.11351*, 2023.
- [28] Christos Louizos, Uri Shalit, Joris M Mooij, David Sontag, Richard Zemel, and Max Welling. Causal effect inference with deep latent-variable models. *Advances in neural information processing systems*, 30, 2017.
- [29] Uri Shalit, Fredrik D Johansson, and David Sontag. Estimating individual treatment effect: generalization bounds and algorithms. In *International Conference on Machine Learning*, pages 3076–3085. PMLR, 2017.
- [30] Siqi Xu, Lin Liu, and Zhonghua Liu. Deepmed: Semiparametric causal mediation analysis with debiased deep learning. *arXiv preprint arXiv:2210.04389*, 2022.
- [31] Lu Cheng, Ruocheng Guo, and Huan Liu. Causal mediation analysis with hidden confounders. In *Proceedings of the Fifteenth ACM International Conference on Web Search and Data Mining*, pages 113–122, 2022.
- [32] Ziqi Xu, Debo Cheng, Jiuyong Li, Jixue Liu, Lin Liu, and Ke Wang. Disentangled representation for causal mediation analysis. *arXiv preprint arXiv:2302.09694*, 2023.
- [33] Oliver Y Chén, Ciprian Crainiceanu, Elizabeth L Ogburn, Brian S Caffo, Tor D Wager, and Martin A Lindquist. High-dimensional multivariate mediation with application to neuroimaging data. *Biostatistics*, 19(2):121–136, 2018.
- [34] Tanmay Nath, Brian Caffo, Tor Wager, and Martin A Lindquist. A machine learning based approach towards high-dimensional mediation analysis. *NeuroImage*, 268:119843, 2023.

- [35] Haixiang Zhang, Jun Chen, Yang Feng, Chan Wang, Huilin Li, and Lei Liu. Mediation effect selection in high-dimensional and compositional microbiome data. *Statistics in medicine*, 40(4): 885–896, 2021.
- [36] Chamila Perera, Haixiang Zhang, Yinan Zheng, Lifang Hou, Annie Qu, Cheng Zheng, Ke Xie, and Lei Liu. Hima2: high-dimensional mediation analysis and its application in epigenome-wide dna methylation data. *BMC bioinformatics*, 23(1):1–14, 2022.
- [37] Tianzhong Yang, Jingbo Niu, Han Chen, and Peng Wei. Estimation of total mediation effect for high-dimensional omics mediators. *BMC bioinformatics*, 22:1–17, 2021.
- [38] Haixiang Zhang, Yinan Zheng, Lifang Hou, Cheng Zheng, and Lei Liu. Mediation analysis for survival data with high-dimensional mediators. *Bioinformatics*, 37(21):3815–3821, 2021.
- [39] Haixiang Zhang, Yinan Zheng, Zhou Zhang, Tao Gao, Brian Joyce, Grace Yoon, Wei Zhang, Joel Schwartz, Allan Just, Elena Colicino, et al. Estimating and testing high-dimensional mediation effects in epigenetic studies. *Bioinformatics*, 32(20):3150–3154, 2016.
- [40] Raymond Hicks and Dustin Tingley. Causal mediation analysis. *The Stata Journal*, 11(4): 605–619, 2011.
- [41] David P MacKinnon, Amanda J Fairchild, and Matthew S Fritz. Mediation analysis. *Annu. Rev. Psychol.*, 58:593–614, 2007.
- [42] James M Robins and Sander Greenland. Identifiability and exchangeability for direct and indirect effects. *Epidemiology*, 3(2):143–155, 1992.
- [43] Paul R Rosenbaum and Donald B Rubin. The central role of the propensity score in observational studies for causal effects. *Biometrika*, 70(1):41–55, 1983.
- [44] Donald B Rubin. Causal inference using potential outcomes: Design, modeling, decisions. *Journal of the American Statistical Association*, 100(469):322–331, 2005.
- [45] Karl Deisseroth. Optogenetics. *Nature Methods*, 8(1):26–29, Jan 2011. ISSN 1548-7105. doi: 10.1038/nmeth.f.324. URL <https://doi.org/10.1038/nmeth.f.324>.
- [46] Patricia Limousin and Tom Foltynie. Long-term outcomes of deep brain stimulation in parkinson disease. *Nature Reviews Neurology*, 15(4):234–242, Apr 2019. ISSN 1759-4766. doi: 10.1038/s41582-019-0145-9. URL <https://doi.org/10.1038/s41582-019-0145-9>.
- [47] Yusuf Tufail, Anna Yoshihiro, Sandipan Pati, Monica M. Li, and William J. Tyler. Ultrasonic neuromodulation by brain stimulation with transcranial ultrasound. *Nature Protocols*, 6(9): 1453–1470, Sep 2011. ISSN 1750-2799. doi: 10.1038/nprot.2011.371. URL <https://doi.org/10.1038/nprot.2011.371>.
- [48] Neil Gallagher, Kyle R Ulrich, Austin Talbot, Kafui Dzirasa, Lawrence Carin, and David E Carlson. Cross-spectral factor analysis. *Advances in neural information processing systems*, 30, 2017.
- [49] David Carlson, Sunil Kumar, and Kafui Dzirasa. Multi-region local field potential recordings during a tail-suspension test. *Duke Research Data Repository*, 2023.
- [50] Amiram D Vinokur, Richard H Price, and Yaacov Schul. Impact of the jobs intervention on unemployed workers varying in risk for depression. *American journal of community psychology*, 23(1):39–74, 1995.
- [51] Martin Huber, Michael Lechner, and Giovanni Mellace. The finite sample performance of estimators for mediation analysis under sequential conditional independence. *Journal of Business & Economic Statistics*, 34(1):139–160, 2016.
- [52] Austin Talbot, David Dunson, Kafui Dzirasa, and David Carlson. Supervised autoencoders learn robust joint factor models of neural activity. *arXiv preprint arXiv:2004.05209*, 2020.
- [53] Adi Ben-Israel. The change-of-variables formula using matrix volume. *SIAM Journal on Matrix Analysis and Applications*, 21(1):300–312, 1999.

A Detailed Proof of Identifiability

The proof of Theorem 4.4 closely resembles the proof presented in [15], which consists of 3 main steps.

Step 1 The first step is to transform the equality of observed data distributions into equality of noise-free distributions using a convolutional trick based on the 1st assumption in Theorem 4.4. Similar to [15], we introduce the volume of a matrix denoted by $\text{vol } A$ as the product of singular values of A . When A is full column rank, $\text{vol } A = \sqrt{\det A^T A}$, and when A is invertible, $\text{vol } A = |\det A|$. We use this matrix volume as a replacement for the absolute determinant of Jacobian [53] in the change of variables formula, which is most useful when the Jacobian is a rectangular matrix ($d < D$). Suppose we have two sets of parameters $(\mathbf{f}, \mathbf{h}, \mathbf{S}, \boldsymbol{\lambda})$ and $(\tilde{\mathbf{f}}, \tilde{\mathbf{h}}, \tilde{\mathbf{S}}, \tilde{\boldsymbol{\lambda}})$ such that $p_{\mathbf{f}, \mathbf{h}, \mathbf{S}, \boldsymbol{\lambda}}(\mathbf{x}, y | \mathbf{u}) = p_{\tilde{\mathbf{f}}, \tilde{\mathbf{h}}, \tilde{\mathbf{S}}, \tilde{\boldsymbol{\lambda}}}(\mathbf{x}, y | \mathbf{u})$. Recall that $\psi = (\mathbf{f}, \mathbf{h}) : \mathcal{Z} \times \mathcal{U} \rightarrow \mathcal{X} \times \mathcal{Y}$ and define the concatenated vector of \mathbf{x} and y as \mathbf{v} . We have:

$$\int_{\mathcal{Z}} p_{\mathbf{S}, \boldsymbol{\lambda}}(z | \mathbf{u}) p_{\psi}(\mathbf{v} | z, \mathbf{u}) dz = \int_{\mathcal{Z}} p_{\tilde{\mathbf{S}}, \tilde{\boldsymbol{\lambda}}}(z | \mathbf{u}) p_{\tilde{\psi}}(\mathbf{v} | z, \mathbf{u}) dz, \quad (11)$$

$$\int_{\mathcal{Z}} p_{\mathbf{S}, \boldsymbol{\lambda}}(z | \mathbf{u}) p_{\epsilon, \xi}(\mathbf{v} - \psi(z, \mathbf{u})) dz = \int_{\mathcal{Z}} p_{\tilde{\mathbf{S}}, \tilde{\boldsymbol{\lambda}}}(z | \mathbf{u}) p_{\epsilon, \xi}(\mathbf{v} - \tilde{\psi}(z, \mathbf{u})) dz. \quad (12)$$

Next, we apply change of variables $\bar{\mathbf{v}} = \psi(z, \mathbf{u})$ on the left hand side (LHS) and $\bar{\mathbf{v}} = \tilde{\psi}(z, \mathbf{u})$ on the right hand side (RHS):

$$\begin{aligned} & \int_{\mathcal{X} \times \mathcal{Y}} p_{\mathbf{S}, \boldsymbol{\lambda}}(\psi|_{\mathcal{Z}}^{-1}(\bar{\mathbf{v}}) | \mathbf{u}) p_{\epsilon, \xi}(\mathbf{v} - \bar{\mathbf{v}}) \text{vol } J_{\psi^{-1}}(\bar{\mathbf{v}}) d\bar{\mathbf{v}} \\ &= \int_{\mathcal{X} \times \mathcal{Y}} p_{\tilde{\mathbf{S}}, \tilde{\boldsymbol{\lambda}}}(\tilde{\psi}|_{\mathcal{Z}}^{-1}(\bar{\mathbf{v}}) | \mathbf{u}) p_{\epsilon, \xi}(\mathbf{v} - \bar{\mathbf{v}}) \text{vol } J_{\tilde{\psi}^{-1}}(\bar{\mathbf{v}}) d\bar{\mathbf{v}}, \end{aligned} \quad (13)$$

where J denotes the Jacobian and recall that $\psi|_{\mathcal{Z}}^{-1}$ is the projection of ψ^{-1} on \mathcal{Z} . Next, we introduce $\tilde{p}_{\mathbf{S}, \boldsymbol{\lambda}, \psi, \mathbf{u}}(\bar{\mathbf{v}}) = p_{\mathbf{S}, \boldsymbol{\lambda}}(\psi|_{\mathcal{Z}}^{-1}(\bar{\mathbf{v}}) | \mathbf{u}) \text{vol } J_{\psi^{-1}}(\bar{\mathbf{v}}) \mathbb{1}_{\mathcal{X} \times \mathcal{Y}}(\bar{\mathbf{v}})$ on the LHS and similarly on the RHS, then, following [15], Equation 13 reduces to:

$$\int_{\mathcal{X} \times \mathcal{Y}} \tilde{p}_{\mathbf{S}, \boldsymbol{\lambda}, \psi, \mathbf{u}}(\bar{\mathbf{v}}) p_{\epsilon, \xi}(\mathbf{v} - \bar{\mathbf{v}}) d\bar{\mathbf{v}} = \int_{\mathcal{X} \times \mathcal{Y}} \tilde{p}_{\tilde{\mathbf{S}}, \tilde{\boldsymbol{\lambda}}, \tilde{\psi}, \mathbf{u}}(\bar{\mathbf{v}}) p_{\epsilon, \xi}(\mathbf{v} - \bar{\mathbf{v}}) d\bar{\mathbf{v}}, \quad (14)$$

$$(\tilde{p}_{\mathbf{S}, \boldsymbol{\lambda}, \psi, \mathbf{u}} * p_{\epsilon, \xi})(\mathbf{v}) = (\tilde{p}_{\tilde{\mathbf{S}}, \tilde{\boldsymbol{\lambda}}, \tilde{\psi}, \mathbf{u}} * p_{\epsilon, \xi})(\mathbf{v}), \quad (15)$$

$$F[\tilde{p}_{\mathbf{S}, \boldsymbol{\lambda}, \psi, \mathbf{u}}](\omega) \varphi_{\epsilon, \xi}(\omega) = F[\tilde{p}_{\tilde{\mathbf{S}}, \tilde{\boldsymbol{\lambda}}, \tilde{\psi}, \mathbf{u}}](\omega) \varphi_{\epsilon, \xi}(\omega), \quad (16)$$

$$F[\tilde{p}_{\mathbf{S}, \boldsymbol{\lambda}, \psi, \mathbf{u}}](\omega) = F[\tilde{p}_{\tilde{\mathbf{S}}, \tilde{\boldsymbol{\lambda}}, \tilde{\psi}, \mathbf{u}}](\omega), \quad (17)$$

$$\tilde{p}_{\mathbf{S}, \boldsymbol{\lambda}, \psi, \mathbf{u}}(\mathbf{v}) = \tilde{p}_{\tilde{\mathbf{S}}, \tilde{\boldsymbol{\lambda}}, \tilde{\psi}, \mathbf{u}}(\mathbf{v}), \quad (18)$$

where we use $*$ for the convolutional operator in Equation 15, we use $F[\cdot]$ to designate the Fourier transform in Equation 16, $\varphi_{\epsilon, \xi} = F[p_{\epsilon, \xi}]$ according to the definition of the characteristic function, and we drop $\varphi_{\epsilon, \xi}(\omega)$ from both sides in Equation 17 as it is non-zero almost everywhere by the 1st assumption in Theorem 4.4.

Equation 18 is valid for all $(\mathbf{v}, \mathbf{u}) \in \mathcal{X} \times \mathcal{Y} \times \mathcal{U}$. It indicates that for the observed data distributions to be the same, the noise-free distributions have to be the same.

Step 2 The second step in [15] is about removing all terms that are either a function of observations \mathbf{x} and y or auxiliary variables \mathbf{u} , which is done by introducing the points provided by the 4th assumption in Theorem 4.4, and using \mathbf{u}_0 as a ‘‘pivot’’. Specifically, by taking the logarithm on both sides of Equation 18 and plugging in Equation 6 for $p_{\mathbf{S}, \boldsymbol{\lambda}}$, we get:

$$\begin{aligned} & \log \text{vol } J_{\psi^{-1}}(\mathbf{v}) + \sum_{i=1}^d \left(\log Q_i(\psi_i^{-1}(\mathbf{v})) - \log C_i(\mathbf{u}) + \sum_{j=1}^k S_{i,j}(\psi_i^{-1}(\mathbf{v})) \lambda_{i,j}(\mathbf{u}) \right) \\ &= \log \text{vol } J_{\tilde{\psi}^{-1}}(\mathbf{v}) + \sum_{i=1}^d \left(\log \tilde{Q}_i(\tilde{\psi}_i^{-1}(\mathbf{v})) - \log \tilde{C}_i(\mathbf{u}) + \sum_{j=1}^k \tilde{S}_{i,j}(\tilde{\psi}_i^{-1}(\mathbf{v})) \tilde{\lambda}_{i,j}(\mathbf{u}) \right). \end{aligned} \quad (19)$$

Let $\mathbf{u}_0, \dots, \mathbf{u}_{dk}$ be the points provided by the 4th assumption of Theorem 4.4, and define $\bar{\boldsymbol{\lambda}}(\mathbf{u}) := \boldsymbol{\lambda}(\mathbf{u}) - \boldsymbol{\lambda}(\mathbf{u}_0)$. Then for $l = 1, \dots, dk$, we plug each of those \mathbf{u}_l in Equation 19 to obtain $dk + 1$ equations and subtract the first equation for \mathbf{u}_0 from the remaining dk equations to get:

$$\langle \mathbf{S}(\boldsymbol{\psi}_{|z}^{-1}(\mathbf{v})), \bar{\boldsymbol{\lambda}}(\mathbf{u}_l) \rangle + \sum_{i=1}^d \log \frac{C_i(\mathbf{u}_0)}{C_i(\mathbf{u}_l)} = \langle \tilde{\mathbf{S}}(\tilde{\boldsymbol{\psi}}_{|z}^{-1}(\mathbf{v})), \bar{\boldsymbol{\lambda}}(\mathbf{u}_l) \rangle + \sum_{i=1}^d \log \frac{\tilde{C}_i(\mathbf{u}_0)}{\tilde{C}_i(\mathbf{u}_l)}, \quad (20)$$

where $\langle \cdot, \cdot \rangle$ denotes inner product. Let L be the matrix defined in the 4th assumption of Theorem 4.4, and \tilde{L} similarly for $\tilde{\boldsymbol{\lambda}}$ (\tilde{L} is not necessarily invertible). Define $b_l = \sum_{i=1}^d \log \frac{\tilde{C}_i(\mathbf{u}_0)C_i(\mathbf{u}_l)}{C_i(\mathbf{u}_0)\tilde{C}_i(\mathbf{u}_l)}$ and \mathbf{b} the vector of all b_l for $l = 1, \dots, dk$. Expressing Equation 20 in matrix form, we get:

$$L^T \mathbf{S}(\boldsymbol{\psi}_{|z}^{-1}(\mathbf{v})) = \tilde{L}^T \tilde{\mathbf{S}}(\tilde{\boldsymbol{\psi}}_{|z}^{-1}(\mathbf{v})) + \mathbf{b}. \quad (21)$$

Multiplying both sides of Equation 21 by the transpose of the inverse of L^T , we get:

$$\mathbf{S}(\boldsymbol{\psi}_{|z}^{-1}(\mathbf{v})) = A \tilde{\mathbf{S}}(\tilde{\boldsymbol{\psi}}_{|z}^{-1}(\mathbf{v})) + \mathbf{c}, \quad (22)$$

where $A = L^{-T} \tilde{L}$ and $\mathbf{c} = L^{-T} \mathbf{b}$. Note that here $\boldsymbol{\psi}_{|z}^{-1}(\mathbf{v})$ can be referred to either the projection from \mathbf{f} or from \mathbf{h} as we map the same Z into \hat{X} and Y through $p_{\mathbf{f}}$ and $p_{\mathbf{h}}$, respectively.

Step 3 In the last step, Khemakhem et al. [15] show that the linear transformation A is invertible for both $k = 1$ and $k > 1$, resulting in an equivalence relation in the iVAE framework. This is mainly based on the 3rd assumption in Theorem 4.4 which guarantees the existence of the $dk \times d$ Jacobian matrix of \mathbf{S} with rank d . This also implies that the Jacobian of $\tilde{\mathbf{S}} \circ \tilde{\boldsymbol{\psi}}_{|z}^{-1}$ exists and is of rank d and so is A . We argue that the proof of invertibility in our framework follows the same line of reasoning as that of the iVAE.

Therefore, with Equation 22 and the invertibility of A , we prove that the parameters $(\mathbf{f}, \mathbf{h}, \mathbf{S}, \boldsymbol{\lambda})$ are \sim_A -identifiable.

B Details of Experimental Setup

Model Configuration In all experiments, the encoder $q_{\phi}(z|\mathbf{x}, \mathbf{u})$, decoder $p_{\mathbf{f}}(\mathbf{x}|z)$, and prior $p_{\mathbf{S}, \boldsymbol{\lambda}}(z|\mathbf{u})$ of IMAVAE are configured as multivariate normal distributions whose mean and covariance are parameterized as a function of the conditioned variables using a feed-forward neural network. As for the predictor $g_{\gamma}(z, \mathbf{u})$, it is implemented as a simple linear regression model. It is worth noting that while alternative stochastic models can also be employed to replace g_{γ} , our experiments demonstrate that the linear regression model already achieves superior performance. See the included code link for details on reproduction of all experiments.

Training Details When training IMAVAE to minimize the objective in Equation 8, we use the Adam optimizer and adopt parameter annealing so that the KL divergence will gradually dominate the reconstruction error in ELBO.

Computing Resources The experiments conducted on the synthetic data and the Jobs II data in Sections 5.1 and 5.3 are of a relatively small scale and can be executed locally. The experiment on the electrophysiological data is performed on a computer cluster equipped with a GeForce RTX 2080 Ti GPU.

Data Availability Multi-region local field potential recordings during a tail-suspension test is an experiment comparing the electrical neural activity and behaviors of Wildtype and Clock- Δ 19 genotypes of mice in the tail-suspension test. This dataset is available to download at <https://research.repository.duke.edu/concern/datasets/zc77sr31x?locale=en> for free under a Creative Commons BY-NC Attribution-NonCommercial 4.0 International license.

Jobs II is a randomized field experiment that investigates the efficacy of a job training intervention on unemployed workers, which can be downloaded from the R package "mediation" or the following URL: <https://r-data.pmagunia.com/dataset/r-dataset-package-mediation-jobs>.

C Synthetic Data Generation

The synthetic data contains $N = 6000$ data points and is generated according to the causal graphs shown in Figure 1. Specifically, for case (a) without observed covariates, we generate t_i , \mathbf{z}_i , \mathbf{x}_i , and y_i for $i = 1, \dots, N$ as follows:

$$\begin{aligned} t_i &\sim \text{Bernoulli}(p), \\ \mathbf{z}_i &\sim \mathcal{N}(\mathbf{0}, \sigma_z^2 \mathbf{I}_d) + c \mathbb{I}(t_i = 1) \mathbf{1}_d, \\ \mathbf{x}_i &= f(\mathbf{z}_i) + \epsilon_x, \\ y_i &= \mu_t t_i + \boldsymbol{\mu}_z^T \mathbf{z}_i + \epsilon_y, \end{aligned}$$

where p is a probability parameter, σ_z^2 is a variance parameter, \mathbf{I}_d is a $d \times d$ identity matrix, $\mathbb{I}(\cdot)$ denotes the indicator function, $\mathbf{1}_d$ is a d -dimensional vector of all ones, $f : \mathbb{R}^d \rightarrow \mathbb{R}^D$ is a nonlinear function modeled by an un-trained neural network, $\epsilon_x \in \mathbb{R}^D$ and $\epsilon_y \in \mathbb{R}$ are Gaussian noise terms, and c , μ_t , and $\boldsymbol{\mu}_z$ are coefficient constants/vector. For case (b) with observed covariates, we generate t_i , \mathbf{z}_i , \mathbf{x}_i , \mathbf{w}_i , and y_i for $i = 1, \dots, N$ as follows:

$$\begin{aligned} \mathbf{w}_i &\sim \mathcal{N}(\mathbf{0}, \sigma_w^2 \mathbf{I}_m), \\ t_i &\sim \text{Bernoulli}(\text{sigmoid}(\boldsymbol{\mu}_s^T \mathbf{w}_i)), \\ \mathbf{z}_i &\sim \mathcal{N}(\mathbf{0}, \sigma_z^2 \mathbf{I}_d) + c_1 \mathbb{I}(t_i = 1) \mathbf{1}_d + c_2 f_1(\mathbf{w}_i), \\ \mathbf{x}_i &= f_2(\mathbf{z}_i) + \epsilon_x, \\ y_i &= \mu_t t_i + \boldsymbol{\mu}_z^T \mathbf{z}_i + \boldsymbol{\mu}_w^T \mathbf{w}_i + \epsilon_y, \end{aligned}$$

where σ_w^2 , σ_z^2 are variance parameters, \mathbf{I}_m , \mathbf{I}_d are identity matrices with dimension $m \times m$ and $d \times d$, respectively, $\mathbb{I}(\cdot)$ denotes the indicator function, $\mathbf{1}_d$ is a d -dimensional vector of all ones, $f_1 : \mathbb{R}^m \rightarrow \mathbb{R}^d$, $f_2 : \mathbb{R}^d \rightarrow \mathbb{R}^D$ are nonlinear functions modeled by un-trained neural networks, $\epsilon_x \in \mathbb{R}^D$ and $\epsilon_y \in \mathbb{R}$ are Gaussian noise terms, and $c_1, c_2, \mu_t, \boldsymbol{\mu}_s, \boldsymbol{\mu}_z, \boldsymbol{\mu}_w$ are coefficient constants/vectors.

D Post-processing for Tail Suspension Test Data

As elaborated in Section 5.2, we have the LFP signals from 26 mice. The full dataset contains a total of $N = 43882$ data points. The observed feature, i.e. \mathbf{x}_i , represents the power spectral densities of the LFPs recorded at 11 brain regions. These densities are evaluated from 1 to 56Hz, resulting in a total of 616 attributes, i.e. $\mathbf{x}_i \in \mathbb{R}^{616}$. We also have treatment assignment t_i indicating whether the mouse corresponding to the i^{th} data point is recorded during an open field exploration ($t_i = 0$) or a tail suspension test ($t_i = 1$).

To generate the semi-synthetic dataset, we do some post-processing on these data. For case (a) without observed covariates, we first apply PCA to map \mathbf{x}_i into a lower-dimensional representation \mathbf{s}_i . Then the true mediator \mathbf{z}_i is generated by $\mathbf{z}_i = \mathbf{s}_i + \mathbb{I}(t_i = 1)$ where $\mathbb{I}(\cdot)$ denotes the indicator function. The final outcome y_i is modeled by $y_i = \mu_t t_i + \boldsymbol{\mu}_z^T \mathbf{z}_i + \epsilon_y$ where $\mu_t, \boldsymbol{\mu}_z$ are coefficient constant/vector and ϵ_y is a Gaussian noise term. For case (b), we use the genotype of the mouse $w_i \in \{0, 1\}$ as an observed covariate where $w_i = 0$ denotes wild type and $w_i = 1$ denotes Clock Δ 19 mutation. The true mediator \mathbf{z}_i is then generated by $\mathbf{z}_i = \mathbf{s}_i + \mathbb{I}(t_i = 1) + f(\mathbf{w}_i)$ where $f : \mathbb{R} \rightarrow \mathbb{R}^d$ is a nonlinear function modeled by a neural network. The final outcome y_i is modeled by $y_i = \mu_t t_i + \boldsymbol{\mu}_z^T \mathbf{z}_i + \mu_w w_i + \epsilon_y$ where $\mu_t, \mu_w, \boldsymbol{\mu}_z$ are coefficient constants/vector and ϵ_y is a Gaussian noise term.

E Simulation Procedure for Jobs II Data

To achieve *zero* direct, mediation, and total effects, we adopt the following simulation procedure, similar to [31, 51], on the Jobs II dataset. Note that all attributes other than T, Z, Y are treated as observed covariates W in this analysis. X in our causal graphs does not exist in this dataset.

1. Estimate probit specifications in which we regress (a) T on W to get an estimated probit coefficient $\hat{\beta}_{\text{pop}}$ and (b) Z on T and W to get estimated probit coefficients $\hat{\gamma}_{\text{pop}}$ and $\hat{\delta}_{\text{pop}}$, respectively.

2. Apply the indicator function to Z so that the mediator becomes a binary variable $Z := \mathbb{I}(Z \geq 3)$.
3. Discard all samples with either $T = 0$ or $Z = 0$, resulting in a dataset with all non-mediated and non-treated samples.
4. Draw independent Monte Carlo samples (500 and 1000 samples for Tables 4 and 5, respectively) with replacement (T', Z', W', Y') from the resulting dataset.
5. Simulate the (pseudo-)treatment and (pseudo-)mediator using the following formula:

$$T' := \mathbb{I}(W' \hat{\beta}_{\text{pop}} + U > 0),$$

$$M' := \eta(T' \hat{\gamma}_{\text{pop}} + W' \hat{\delta}_{\text{pop}}) + \alpha + V,$$

where $U \sim \mathcal{N}(0, 1)$, $V \sim \mathcal{N}(0, 1)$, η is a simulation parameter which stands for the magnitude of selection into the mediator, and we manually set α such that either 10% or 50% of the samples are mediated (i.e. $M' \geq 3$). Note that here the (pseudo-)mediator M' is continuous after simulation.

With this simulation design, the ground truth of the direct, mediated, and total effects are all *zero*.